Journal of Nuclear Materials 406 (2010) 55–67

Contents lists available at ScienceDirect

Journal of Nuclear Materials

journal homepage: www.elsevier.com/locate/jnucmat

Atomistic Kinetic Monte Carlo studies of microchemical evolutions driven by diffusion processes under irradiation

F. Soisson [a,*], C.S. Becquart [b], N. Castin [c], C. Domain [d], L. Malerba [c], E. Vincent [d,e]

[a] Service de Recherches de Métallurgie Physique, CEA Saclay, 91191 Gif-sur-Yvette, France
[b] Unité Matériaux Et Techniques (UMET), UMR 8207, Université Lille-1, F-59655 Villeneuve d'Ascq Cedex, France
[c] Structural Materials Group, Nuclear Materials Science Institute, SCK•CEN, Boeretang 200, B 2400 Mol, Belgium
[d] EDF-R&D Département MMC, Les Renardières, F-77818 Moret-sur-Loing Cedex, France
[e] Laboratoire de Métallurgie Physique et Génie des Matériaux, UMR 8517, Université Lille-1, F-59655 Villeneuve d'Ascq Cedex, France

A B S T R A C T

Atomistic Kinetic Monte Carlo (AKMC) simulations are a powerful tool to study the microstructural and microchemical evolution of alloys controlled by diffusion processes, under irradiation and during thermal ageing. In the framework of the FP6 Perfect program, two main approaches have been applied to binary and multicomponent iron based alloys. The first one is based on a diffusion model which takes into account vacancy and self-interstitial jumps, using simple rigid lattice approximation and broken-bond models to compute the point-defect jump frequencies. The corresponding parameters are fitted on *ab initio* calculations of a few typical configurations and migration barriers. The second method uses empirical potentials to compute a much larger number of migration barriers, including atomic relaxations, and Artificial Intelligence regression methods to predict the other ones. It is somewhat less rapid than the first one, but significantly more than simulations using "on-the-fly" calculations of all the barriers. We review here the recent advances and perspectives concerning these techniques.

1. Introduction

On the nanosecond scale, the modelling of radiation damage in metallic materials by classical molecular dynamics (MD) is very efficient [1]. The creation of point defects in displacement cascades, their recombination, the formation of small point defect clusters and their interaction with other clusters or solute atoms, are simulated by a direct numerical integration of the Newtonian equations of motion. The key issue is then to use interatomic potentials which correctly reproduce the physical properties of the materials one wishes to simulate. In the case of α-iron for example, important results have been achieved recently, thanks to the development of significantly better potentials, being especially able to reproduce the self-interstitial atoms (SIAs) properties predicted by *ab initio* results [2].

However, MD simulations must use time steps much smaller than the time scale of lattice vibrations (typically $\sim 10^{-15}$ s). The microstructure and microchemical evolutions in structural materials of nuclear reactors are controlled by processes of solute diffusion, solute and point defect clustering, solute segregation or precipitation, etc. that take place over decades. These phenomena are driven by thermally activated jumps of point defects, with activation energies between a few tenths of and a few eV. As a consequence it is clear that, at ordinary operating temperatures, the long range diffusion of atoms and the long term microstructural and microchemical evolutions are not in the range of MD simulations.

In the Atomistic Kinetic Monte Carlo (AKMC) simulations presented here, the elementary mechanisms are not the lattice vibrations, but the point-defect jumps. The key point that guarantees the correct modelling of the kinetic pathways of a given system, either during thermal ageing or under irradiation, is a realistic description of diffusion mechanisms and rates (this also includes the information on the *thermodynamic* properties of the materials). The Monte Carlo simulations performed in the framework of the PERFECT Project (henceforth *the Project*) are all based on this idea, but they differ by the compromise between the realism of the description and the computing cost. The choice of the good compromise is delicate and dictated by the precise problem and system under consideration. In the following, we review the studies carried out in the framework of the Project. After a brief description of the different methods, we will present some significant results, with special emphasis on iron–copper based and other ferritic alloys.

2. Atomistic Kinetic Monte Carlo methods

In AKMC models, the complete atomic configurations of finite size systems (with typically between 10^5 and 10^7 atoms) is

* Corresponding author. Tel.: +33 1 69 08 27 67; fax: +33 1 69 08 68 67.
E-mail address: frederic.soisson@cea.fr (F. Soisson).

0022-3115/$ - see front matter © 2010 Elsevier B.V. All rights reserved.
doi:10.1016/j.jnucmat.2010.05.018

considered. They are then in principle more realistic (and more time consuming) than other simulation techniques that only consider some predefined "objects" (solute atoms or defects, and their clusters), such as rate theory or cluster dynamics, Event KMC and Object KMC (see Ref. [3]). In particular, AKMC techniques are the only ones capable of tracing as correctly as possible the microchemical evolution of the system, irrespective of the concentration of solute elements.

2.1. Diffusion models

In AKMC simulations, the atomic configuration evolves by point-defect jumps i, occurring with thermally activated frequencies:

$$\Gamma_i = \nu_i \exp(-\Delta E_i^m / k_B T). \quad (1)$$

In this expression, ν_i is usually called the "attempt frequency" and ΔE_i^m the activation energy or "migration barrier" of the jump. Such a description is derived from the theory of thermally activated processes, and is justified when the thermal fluctuations are smaller than the activation energies ($k_B T \ll \Delta E_i^m$). During thermal ageing of substitutional alloys, the most common diffusion mechanism is the vacancy jump. Over the last few years, many AKMC studies have been devoted to the modelling of thermal ageing in binary, ternary and even multicomponent alloys, and to the effects of the vacancy diffusion mechanisms [4–26]. A few simulations also take into account the diffusion of small elements by a direct interstitial mechanism (such as carbon in steels [27–29]).

One of the main achievements of the Project has been the development of diffusion models and Monte Carlo algorithms that explicitly take into account radiation induced diffusion mechanisms, including the migration of SIAs, with their specific configurations and migration path. The typical case is the translation–rotation jump of $\langle 1\,1\,0\rangle$ dumbbells, in bcc iron and iron based alloys [30–33]. However, the studies of the consequences of these diffusion mechanisms on the evolution of alloys under irradiation are only beginning and some phenomena (such as SIA clustering) are not yet properly treated.

Another merit has been emphasising the importance of accounting as correctly as possible, in the AKMC simulations, for the dependence of the migration barrier on the local chemical configuration. Doing so in a rigorous way is far from trivial and the work performed during the Project shows that different descriptions of this dependence determine sometimes dramatic differences on the simulated kinetics [11,19,34].

2.2. Monte Carlo algorithms

All of the AKMC simulations presented here use similar Residence Time, or Continuous Time algorithms [35,36] to realize the point-defect jumps. At each Monte Carlo step, the N_J possible jumps are determined and their respective jump frequencies Γ_i are computed. One of the jumps is chosen, using a pseudo-random number, with a probability proportional to its jump frequency.

The Residence Time algorithm requires the evaluation of the frequency of all the migration events at each step, but guarantees that one jump is always performed (no null event). In the case of the diffusion by point-defect jumps there are only a few possible events (in α-iron for example, a vacancy can jump toward eight nearest-neighbour sites and a $\langle 1\,1\,0\rangle$ dumbbell toward four nearest-neighbour sites, see Section 3.1). Schemes of this type are usually much more efficient than Metropolis-like algorithms [22], in which the possibility that the chosen event is rejected exists [37]. The time increment associated to the Monte Carlo step is given by:

$$t = \left(\sum_{i=1}^{N_J} \Gamma_i \right)^{-1} \quad (2)$$

The same algorithm can deal with the formation of Frenkel pairs and displacement cascades (the corresponding frequencies are directly given by the radiation dose rate, in dpa s^{-1}) and with point defects recombination and annihilation at sinks. These athermal events occur instantaneously, adding no contribution to the time in Eq. (2). More information can be found in Refs. [19,33,38,39].

2.3. Migration barriers

The migration barriers ΔE_i^m and the attempt frequencies ν_i contain all the thermodynamic and kinetic information on the system. Their dependence on the local atomic configuration controls the correlation effects, the diffusion properties, the chemical fluxes and finally the kinetic pathway of the system.[1] Even for binary alloys, the number of possible configurations and barriers increases very rapidly with the range of interactions [34]. Several approaches can be used to estimate the barriers, here briefly summarized.

2.3.1. Rigid lattice approximation with effective interaction energies

The total system energy is computed, in most cases, as a sum of constant pair interactions ε_{ij} between i and j neighbouring atoms on a perfect lattice, with no relaxation. Vacancy–atom interactions ε_{iV} are used to reproduce the vacancy formation and the vacancy–solute binding energies [11,16,18,19,21]. The energetic properties of SIAs can also be reproduced in such a framework: it has been done for the $\langle 1\,1\,0\rangle$ dumbbells if Fe–Cu dilute atoms by introducing effective dumbbell–atom interactions [38,40], or by directly incorporating the DFT binding energies in the migration barriers [19,33,39]. Both methods take into account pure and mixed dumbbells configurations and their anisotropic interactions with neighbouring atoms located on compression or tension sites (Fig. 1). N-body interactions (triangle, tetrahedron, etc. interactions) can also be taken into account to improve the description of the configuration energies [41,42], but this increases the computation time [41,42]. Alternatively, the total energy can be calculated with a many-body interatomic potential, still without including relaxation effects [22–26].

The migration barriers can be computed using various "broken-bond" models, whose parameters have to be fitted on experimental measurements, empirical potentials or – more and more often – *ab initio* calculations. Two models have been commonly used in the framework of the Project: the Kinetic Ising Model (KIM, also called FISE in Ref. [21], for Final–Initial System Energy) and the Saddle-Point Energy Model, which differ by the way they introduce the dependence of the barriers on the local environment. More details are given in Appendix A.

In spite of their inherent limitations, these methods have the great advantage of being computationally very rapid ($\sim 10^6$ jumps per second can be performed) and simple enough to be directly compared with analytical models, such as diffusion models for the computation of diffusion coefficients, classical nucleation-growth and coarsening models for the kinetics of precipitation, etc. They have been used to study the kinetics of precipitation in iron–copper and other iron based alloys, both during thermal ageing and under irradiation: these studies are presented in Section 3. Their main limitation is the rigid lattice approximation itself and the fact that they are based on oversimplified interaction models, with few parameters fitted only on a small number of configurations and barriers. The extrapolation to other ones can be very dependent on the system under consideration.

[1] Most studies pay much more attention to the description of the migration barriers than to the attempt frequencies ν_i, because of the exponential dependence of the jump frequencies on ΔE_i^m. Nevertheless, the attempt frequencies should also depend on the local configuration, with possible effects on the kinetic pathways.

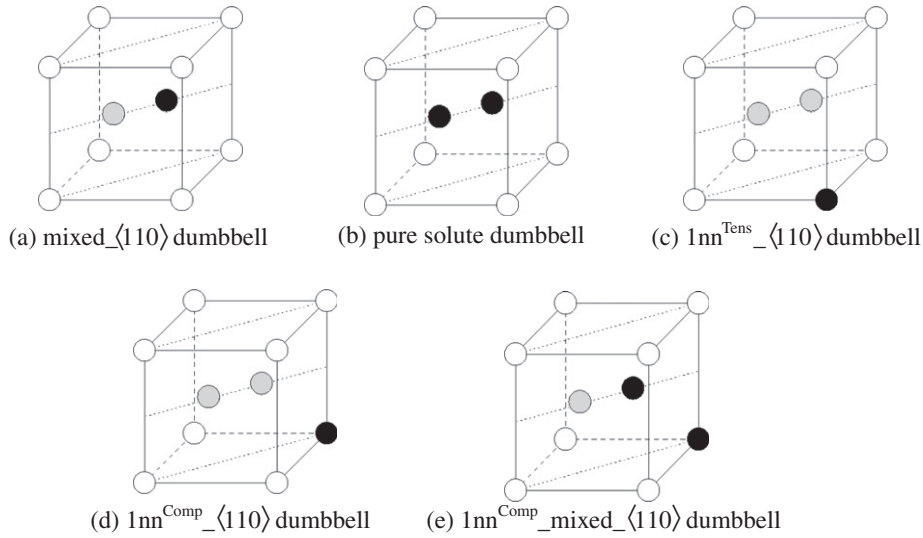

Fig. 1. ⟨1 1 0⟩ dumbbell–solute configurations in bcc iron. The black circles correspond to the solute atoms, the grey ones to the Fe atoms within the dumbbell and the white circles to the Fe atoms in the matrix, outside the dumbbell. The configuration (c) is under tension, whereas (a), (b), (d) and (e) are under compression.

2.3.2. On-the-fly calculations with atomic relaxations

On the opposite side, some AKMC schemes use "on-the-fly" computation of the migration barriers with interatomic potentials, including atomic relaxations. The relaxation of atomic positions can be performed using conjugate gradient (CG), molecular statics (MS) or Monte Carlo techniques [43–45]. Several algorithms exist that allow the energy barrier to be calculated, the most widespread ones being the drag, the nudged elastic band (NEB) and the dimer methods [46]. All of them correspond to increasingly refined strategies to find the saddle point of the system along the transition between initial and final states. Drag and NEB methods require the knowledge of both states, the latter being more precise (and computationally demanding) than the former, while the dimer method is designed to search all possible saddle points from a given initial state. In practice, for actual on-the-fly calculations, only the drag method has been used [44]. The most complete simulations include the computation of the attempt frequencies from the vibration eigenmodes, in the harmonic approximation, in addition to the complete relaxation of stable and saddle-point positions [44].

The main advantage of on-the-fly calculations is that not only chemical, but also long range elastic interactions are taken into account, thereby including their effect on the formation of precipitates and defect clusters. These schemes are, however, still computationally too heavy to be applied in microstructure evolution studies and are therefore only of use, in a limited number of cases, for the study of simple species diffusion properties. Further approximations are otherwise required to accelerate the computation of the barriers, such as limiting the relaxation in a given volume only. Simpler diffusion mechanisms (e.g. direct exchanges between atoms) can be used to avoid strong trapping and correlation effects [43].

2.3.3. Advanced regression methods

Another possibility is to use advanced regression methods, fitted to a suitable number of examples, to substitute direct barrier calculations, including relaxations, with a formula that provides the correct dependence of the barriers on the local environment, both in terms of chemical configuration and strain field. One of the objectives of the Project was therefore the development of such an alternative method, using artificial intelligence (AI) regression techniques: recent progress and applications to iron–copper alloys are presented in Section 4.

3. Precipitation in dilute iron–copper alloys in rigid lattice approximations

The ageing of bcc iron based alloys, with small contents of copper and other solutes (Ni, Mn, Si, etc.), is of special importance in the nuclear industry. The formation of copper-rich clusters, accelerated or induced by irradiation, has long been suspected to play a key role in the hardening and embrittlement of some pressure vessels steels and many experimental studies have been devoted to this problem (see, e.g., Ref [47]).

The size misfit between copper and iron lattices is small and during the first stage of precipitation under thermal ageing, copper precipitates remain fully coherent with the α-iron bcc matrix, until precipitate radii of approximately 2 nm [48]. AKMC simulations based on rigid lattice approximations are thus well suited to model the early stages of copper precipitation, and several studies have been proposed over the last decade [7,11,15,16,19–21].

3.1. Ab initio calculations for the parameterization of AKMC simulations

The first AKMC simulations of copper precipitation were based on rigid lattice approximations and simple broken bonds models (see Appendix A), using experimental data [7,15,16,20] or empirical interatomic potentials [11] to determine the parameters involved in the jump frequencies. But the available experimental results are often limited and the reliability of empirical potential is questionable to predict quantities that have not been explicitly taken into account in their development (for a discussion on the advantages and limitations of current empirical potentials, see below, Section 4.1). Among the difficult points are the copper solubility limit, which was until recently only known at high temperature (above 700 °C) [49]. Recent results have shown that the extrapolation of such data below 500 °C leads to an underestimation of the copper solubility [50]. Concerning the diffusion properties, only the iron self-diffusion and the copper impurity diffusion coefficients are known, again at high temperature [49,50]. Moreover, the properties of bcc copper-rich precipitates (solubility of iron, point defect formation energies and diffusion properties) are of course very difficult to measure, since pure copper is fcc.

First principle calculations in the framework of the density functional theory (DFT) provide the most reliable information

today available on these properties and they have been systematically used in the Project [16,18,21,31,51]. Table 1 gives for example a few properties of bcc pure metals and bcc iron- and copper-rich solid solutions: mixing or solution energies of a solute X (E_X^{sol}) *in the matrix, binding energy of X and Y between nth neighbour positions* ($E_{XY}^{b(n)}$) *and vacancy formation energies* (E_V^{for}). The system is characterized by strong unmixing energies (high mixing energies of Cu in Fe and of Fe in Cu, strongly attractive Cu–Cu binding energies in iron). Other features have some special importance: (i) the vacancy formation energy is much larger in bcc iron (more than 2 eV) than in bcc copper (less than 1 eV), which leads to a strong trapping of vacancies in precipitates and (ii) there is a strong attraction between Cu and vacancies in iron, up to the second nearest neighbour position, which leads to a positive coupling between copper and vacancy fluxes [40,52]: the consequences on the microstructure evolution under irradiation will be discussed later (Section 3.3).

In addition to the thermodynamic properties presented above, some vacancy migration barriers have been computed using DFT calculations, for various local copper distributions, in order to fit the saddle-point binding energies [16]. In multicomponent alloys, DFT calculations [18] have been used in a similar fashion to compute the binding energies between different solute atoms in iron (Cu, Mn, Ni, Si) and the migration barriers of vacancy solute atoms (Table 2).

For the time being DFT methods are almost the only way to get reliable information on the self-interstitial configurations in alloys that can be used to choose the corresponding AKMC parameters. It has been shown that the most stable configuration in pure bcc iron is the ⟨1 1 0⟩ dumbbell, that diffuses with a rotation towards nearest-neighbour sites and a migration energy of approximately 0.3 eV [31,32]. Interactions of ⟨1 1 0⟩ dumbbells with solute atoms (Cu, Ni, Mn, Si) have been studied in Ref. [30]: mixed Fe–solute dumbbells are not energetically favoured, except in the case of Mn (see Fig. 1 and Table 3). The ⟨1 1 0⟩ configuration remains the most stable in dilute Fe–Cu alloys [30,40], but in pure bcc copper the only DFT calculations that have been performed indicates that the ⟨1 1 1⟩ crowdion configuration is slightly more stable [40].

Migration barriers of self-interstitial atoms have been also computed, in dilute iron alloys [30]. Fig. 2 shows for example the energetic barriers that an interstitial, associated with one Mn atom, has to cross for different configurations. It clearly appears that the mixed ⟨1 1 0⟩ dumbbell is stable and that the translation–rotation jump is also the most favourable jump. Whatever the solute atom, this jump is usually one of the easiest jumps.

Table 1
Thermodynamic properties of vacancies and solute in bcc iron and bcc copper (*ab initio* calculations with 54 sites and relaxation at constant volume, using SIESTA [16]). Comparison with previous results with VASP (USPP) [31].

Energy (eV)	SIESTA	VASP
In bcc iron		
e_{Cu}^{sol}	0.48 (ref: bcc Cu)	
	0.52 (ref: fcc Cu)	0.50–0.55 (ref: fcc Cu)
$E_{CuCu}^{b(1)}$	0.15	0.16
$E_{CuCu}^{b(2)}$	0.03	0.05
$E_{CuV}^{b(1)}$	0.17	0.17
$E_{CuV}^{b(2)}$	0.18	0.19
E_V^{for}	2.18	1.95
In bcc copper		
E_{Fe}^{sol}	0.77	–
$E_{FeFe}^{b(1)}$	0.40	–
$E_{FeFe}^{b(2)}$	0.27	–
$E_{FeV}^{b(1)}$	−0.05	–
$E_{FeV}^{b(2)}$	−0.06	–
E_V^{for}	0.88	–

Table 2
Solution energies, binding energies and migration barriers for vacancy jumps of solute atoms in multicomponent iron based alloys. The calculations have been done using VASP, in the USPP with 128 atom supercells and 3 × 3 × 3 k points [19].

	Cu	Mn	Ni	Si
E_X^{sol} (eV)	0.55	−0.16	−0.17	−1.09
$E_{X-X}^{b(1)}$ (eV)	0.16	−0.20	−0.10	−0.32
$E_{X-X}^{b(2)}$ (eV)	0.05	−0.18	−0.02	−0.18

Energy (eV)	Mn	Ni	Cu
$E_{Si-X}^{b(1)}$	−0.03	0.00	0.06
$E_{Si-X}^{b(2)}$	−0.36	−0.12	−0.05
$E_{Mn-X}^{b(1)}$		−0.12	0.02
$E_{Mn-X}^{b(2)}$		−0.12	−0.07
$E_{Ni-X}^{b(1)}$			0.02
$E_{Ni-X}^{b(2)}$			−0.01

	Fe	Cu	Mn	Ni	Si
ΔE_{mig} (X) (eV)	0.62	0.54	1.03	0.68	0.42

It must be emphasized that key properties given by *ab initio* calculations can usually be reasonably reproduced in a broken-bond model on rigid lattice, especially when atomic relaxations are not too large and at least for some limited range of composition. But such models impose some limitations: for example the use of pair interactions leads to symmetrical thermodynamic properties (e.g. symmetrical phase diagrams) and to other relations between quantities (solute mixing energies and binding energy between solute atoms, solute–vacancy binding and vacancy formation energies, etc.) that are not always fulfilled, even for relatively simple systems such as Fe–Cu alloys [42]. Therefore, the fitting procedure and the resulting AKMC parameters for a given system can differ depending on the problem under consideration (alloy composition, thermal ageing or irradiation conditions).

3.2. Kinetics of copper precipitation: thermal ageing

3.2.1. Thermal ageing of binary Fe–Cu alloys

The recent AKMC simulations of copper precipitation in bcc iron, performed within the Project using different Monte Carlo and DFT codes, are (at least qualitatively) in agreement [16,21].

A common point to these AKMC simulations and to previous ones [7,15], is that the precipitates are almost pure copper since the beginning of the precipitation (even for size of ∼1 nm), which can be explained by the low iron solubility in bcc copper and a diffusion more rapid in bcc copper than in the iron matrix, due to the higher vacancy concentrations.

Fig. 3 gives an example of precipitation kinetics, during a thermal ageing of a Fe–1.34at.%Cu alloy at 550 °C [16]. The simulation gives an evolution of the precipitate size and density in good agreement with the experimental results, but limited to short simulation times and precipitate sizes. This is due to the intrinsic slowness of the AKMC methods, which requires many vacancy jumps (typically a few billions) to reach the early stage of coarsening, especially with the parameters used in Ref. [16] which induce a strong trapping of vacancies in the copper clusters (as shown by the evolution of fraction of time spent by a vacancy in the iron matrix, Fig. 3a). Note that simulations of thermal ageing are usually performed with a constant number of vacancies in the simulation box (typically one). The Monte Carlo time given Eq. (1) must then be rescaled by a ratio $C_v^{MC}(Fe)/C_v^{eq}(Fe)$, where $C_v^{MC}(Fe)$ and $C_v^{eq}(Fe)$

Table 3
Solute(s)-dumbbell complexes binding energies obtained with 54 and 128 atom supercells. The configurations explored are illustrated in Fig. 1. For Mn, the antiferro-magnetic (*af*) or ferro-magnetic (*f*) states are indicated [30].

Binding energy (eV)	Fe–Cu		Fe–Ni		Fe–Mn		Fe–Si	
Supercell size (atoms)	54	128	54	128	54	128	54	128
Mixed-⟨1 1 0⟩ dumbbell	−0.53	−0.46	−0.36	−0.36	0.36 *af*	0.37 *af*	−0.05	0.01
Pure solute dumbbell	−0.50	−0.36	−0.40	−0.30	0.44 *af*	0.47 *af*	−0.58	−0.40
$1nn^{Tens}$-⟨1 1 0⟩ dumbbell	0.06	0.07	−0.14	−0.13	−0.36 *f*	−0.36 *f*	−0.26	−0.23
$1nn^{Comp}$-⟨1 1 0⟩ dumbbell	−0.03	−0.01	−0.06	−0.06	0.09 *af*	0.10 *af*	0.24	0.27
$1nn^{Comp}$-mixed⟨1 1 0⟩dumbbell	−0.26	−0.18	−0.31	−0.32	0.28 *af*	0.29 *af*	−0.54	−0.50

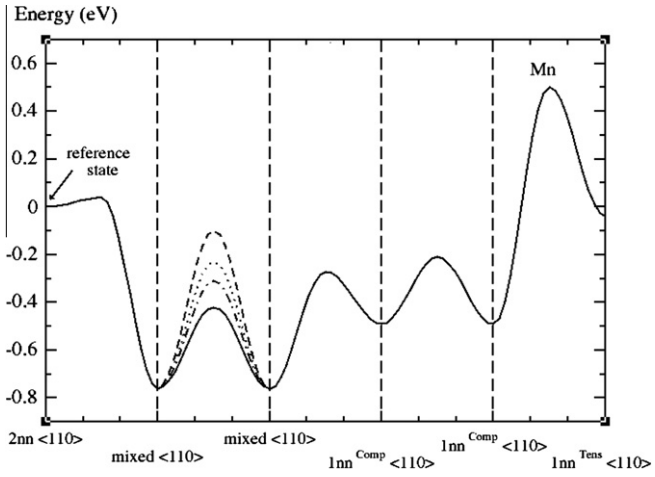

Fig. 2. Dumbbell migration barriers in the vicinity of a Mn atom in bcc iron. For the mixed to mixed dumbbell migration, the four possible jumps are represented: the first nearest neighbour jump combining a translation and a rotation is represented by the continuous line, the first nearest neighbour translation jump by the dashed line. The second nearest neighbour jump combining a translation and a rotation by the dotted line and the rotation jump is represented by the dashed-dotted line [30].

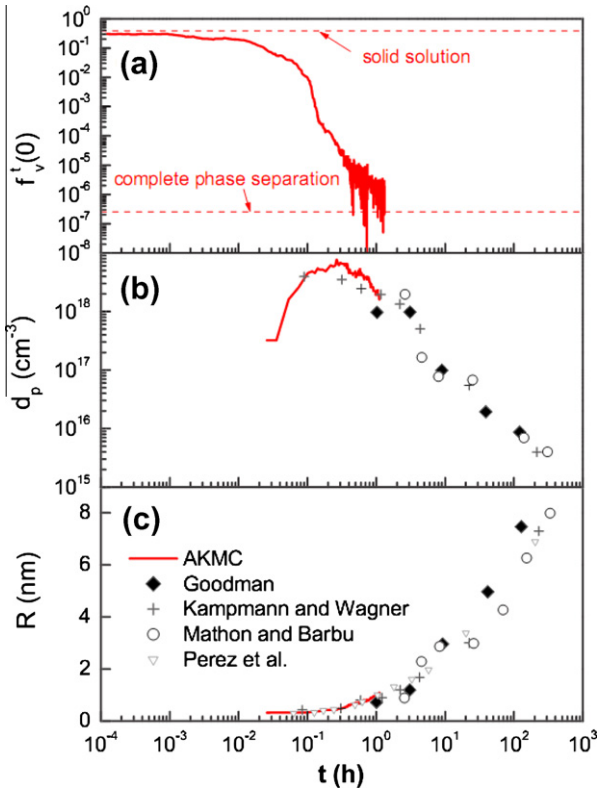

Fig. 3. Monte Carlo simulation of the precipitation kinetics in Fe–1.34 at.% Cu during thermal ageing at 550 °C [16]. Evolution of (a) the fraction of time spent by the vacancy in pure iron, (b) the density of precipitates, and (c) the precipitate radius. The solid lines correspond to the simulations and the symbols to experimental studies (see references in [16]).

are the vacancy concentrations in pure iron, in the Monte Carlo simulations and at equilibrium, respectively. To get a physical time scale it is important to take into account the trapping of the vacancy in the copper cluster, which results in a decrease of C_v^{MC}(Fe) during the precipitation [11,16,21].

A key parameter governing the precipitation kinetics is E_{Cu}^{sol}, the mixing (or solution) energy of copper in iron [21]. DFT calculations [16,31] predict values between 0.48 and 0.55 eV, lower than the one used in previous AKMC studies ($E_{Cu}^{sol} = 0.68$ eV in [15], 0.80 eV in [11], 0.83 eV in [18]), but similar to the one of Schmauder and Binkele ($E_{Cu}^{sol} \sim 0.515$ eV [20]).

A detailed comparison between AKMC simulations performed using different sets of parameters and different models of migration barriers (see Appendix A) can be found in Ref. [21]. The main conclusion is that the simulations performed with E_{Cu}^{sol}(Fe) ~ 0.5 eV show a much lower density of copper precipitates during the nucleation stage, which coarsens more rapidly, than with the parameters of Refs. [11,15], and are overall in better agreement with experimental results. An example is given in Fig. 4, for the Fe–0.6at.%Cu alloy aged at 500 °C [21].

The model chosen to compute the migration barrier (i.e. the first model of Appendix A, which includes a constant migration barrier, corrected by the difference between the final and the initial energy of the system and the second model, with a constant saddle-point energy for jumping atoms) has a significant, but overall lesser effect on the evolution of density and size of precipitates [21]. However, the saddle-point energy dependence on the local configuration does affect the actual kinetic pathway [11].

The importance of the vacancy trapping in Cu-rich clusters differs according to the set of AKMC parameters used in different studies. The stronger effect is observed with parameters derived from DFT calculations performed with the SIESTA code, which predict a vacancy formation energy of more than 2 eV in bcc iron and less than 1 eV in bcc copper (Table 1 and Ref. [16]). An important consequence of this is the high mobility of copper clusters (including several tens of copper atoms), which can diffuse more rapidly than Cu monomers. This mobility is lower if the difference in vacancy formation energy decreases, but seems to be present in most of the AKMC simulations of copper precipitations [7,11,15], and other systems when the vacancies are trapped in the precipitates or at the interface between the precipitates and the matrix [5,17,53].

3.2.2. Thermal ageing of a Fe–CuNiMnSi alloy

The AKMC parameterisation for Fe–CuNiMnSi alloys under ageing conditions was built progressively: first for binary, then ternary and finally quaternary alloys. No detailed experimental studies of

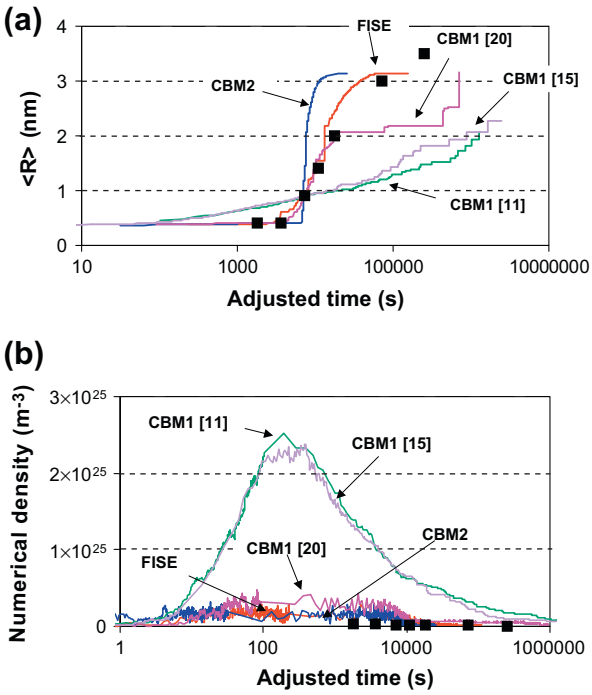

Fig. 4. Comparison between the precipitation kinetics obtained with three models of migration barriers and different sets of AKMC parameters, for the Fe–0.6 at.% Cu alloy aged at 500 °C. (a) Evolution of the Cu cluster mean radius, compared with experiments (black squares), (b) evolution of the numerical density of Cu clusters, compared with experiments (black squares). FISE refers to the model 1 of Appendix A, using parameters of Ref. [21], CBM1 to the model 2, with constant saddle-point energies e_{SP}^{Fe} and e_{SP}^{Cu} and with parameters of Refs. [11,15,20].

thermal ageing are available for the different binary alloys (except for the FeCu system, as presented above). Nevertheless, the tendencies of precipitation have been tested for the Fe–Mn, Fe–Ni and Fe–Si alloys with the *ab initio* obtained parameters (Section 3.1), as compared with the corresponding phase diagrams and adjusted in function.

For the more complex ternary (FeCuNi) and quaternary alloys (FeCuMnNi and FeCuMnSi) thermal ageing experimental results can be found and were used to adjust the other AKMC parameters [19].

AKMC simulations of thermal ageing of a Fe–0.2Cu0.63-Si1.26Mn0.53Ni (in at.%) were performed at 573 and 773 K (see Fig. 5 and Ref. [18]). This composition is close to that of French reactor pressure vessel steels, except for the high Cu concentration. At 573 K (Fig. 5a), only small clusters with less than 10 solute atoms are formed after a thermal ageing of 10 years (the microstructure remains almost the same after 100 years). At 773 K, the microstructure after 10 years of thermal ageing is radically different (Fig. 5b): the simulation displays small Mn–Si ordered precipitates (with a maximum of 8 Mn and 8 Si atoms), small pure copper and bigger precipitates with a copper-rich core surrounded by some Ni, Mn and/or Si atoms. The formation of the latter precipitates is coherent with the thermodynamic data, as was explained by Liu et al. [54]: the segregation of Ni, Mn and Si atoms at the Fe–Cu interface can be explained by the decrease of the interface energy.

3.3. Microstructure evolution under irradiation

3.3.1. Coupling between fluxes, radiation induced segregation and precipitation

Under permanent irradiation conditions, excess point defects can be eliminated by recombination or by diffusion towards available sinks (grain boundaries, dislocations, surfaces, etc.). Irradiation can thus sustain fluxes of point defects and then fluxes of chemical elements, in opposite or alike directions. The composition can be accordingly modified near the sinks: as a matter of fact, radiation induced segregation (RIS) phenomena are quite common in metallic alloys (see, e.g. Ref. [55]). If the local solute concentration reaches the solubility limit, one can then observe radiation induced precipitation, even in an undersaturated solid solution.

The RIS is usually modelled using generalized diffusion equations in the framework of the phenomenological theory of diffusion [56], but the coupling coefficients (the phenomenological coefficients L_{ij} of the Onsager matrix) are difficult to compute from jump frequencies, especially in concentrated alloys and for the dumbbell diffusion mechanisms [56]. Moreover, such models only predict the segregation kinetics, not the precipitation ones.

AKMC simulations have been developed to overcome these difficulties: they take into account the creation of vacancies and SIAs, with a rate given by the impinging radiation flux, their migration, their annihilation at sinks or by mutual recombination [38]. It has been shown that RIS kinetics could be simulated in realistic

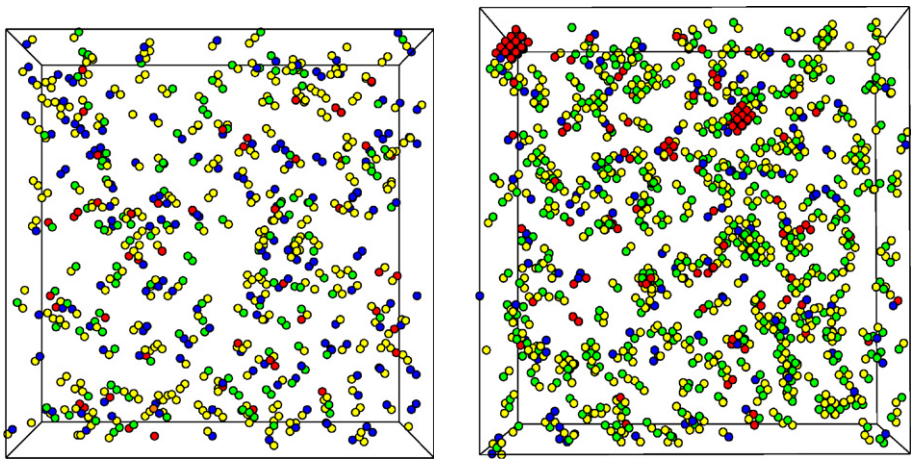

(a) 573 K. t = 10 years (b) 773 K. t = 10 years

Fig. 5. Cluster distributions after thermal ageing of a Fe–0.2Cu0.63Si1.26Mn0.53Ni (in at.%) at 573 and 773 K. The vacancy is black, the Cu atoms appear in red, the Mn ones in yellow, the Si ones in blue and the Ni atoms are green. Only the solute atoms belonging to a cluster are represented. (For interpretation of the references to colour in this figure legend, the reader is referred to the web version of this article.)

irradiation conditions (of flux, temperature, point defect concentrations) and simple model cases have been chosen to test the simulations by quantitative comparisons with rate theory models, and to study the effect of the point defect diffusion properties on the evolution of precipitation microstructure. An example is shown in Fig. 6: the AKMC parameters have been chosen to give a rapid diffusion of B atoms by interstitial diffusion and a rapid diffusion of A atoms by vacancy diffusion. In this undersaturated alloy, inverse Kirkendall effect induces first an enrichment of B atoms near the point defect sink located in the middle of the simulation box, then a precipitation of B when the local concentration reaches the solubility limit.

Similar simulations, taking into account the ⟨1 1 0⟩ dumbbell configurations, have been applied to dilute Fe–Cu alloys, using *ab initio* calculations to fit the AKMC parameters [19,40] (see Section 3.1). In Ref. [40], the phenomenological coefficients which control the coupling between fluxes of Cu and point defects have been measured in the simulations, using the Einstein–Smoluchowski relations [53]:

$$L_{ij} = \frac{1}{Vk_BT}\frac{\langle \mathbf{R}_i.\mathbf{R}_j\rangle}{6t}, \tag{3}$$

where $\mathbf{R}_i$ and $\mathbf{R}_i$ are the displacements of species i and j and V the volume of the system (Fig. 7). At low temperature, the vacancy can drag the copper atoms towards the sinks, because of the strong attractive Cu–V binding up to the second nearest neighbour positions (as already shown by Barashev and Arokiam in the infinite dilution limit [52]). This drives a small enrichment of copper near the sinks. At high temperature, the Cu–V pairs dissociate and Cu and vacancy fluxes are in opposite directions, leading to a copper depletion near the sinks. The coupling between fluxes of copper and interstitial has been found to be negligible. Preliminary simulations of highly supersaturated alloys (copper constant ~1at.%), show that these radiation induced segregations remain limited, and that precipitation kinetics are similar to the ones observed during thermal aging, except for the acceleration due to the point defect supersaturation. Work is in progress to study more diluted alloys.

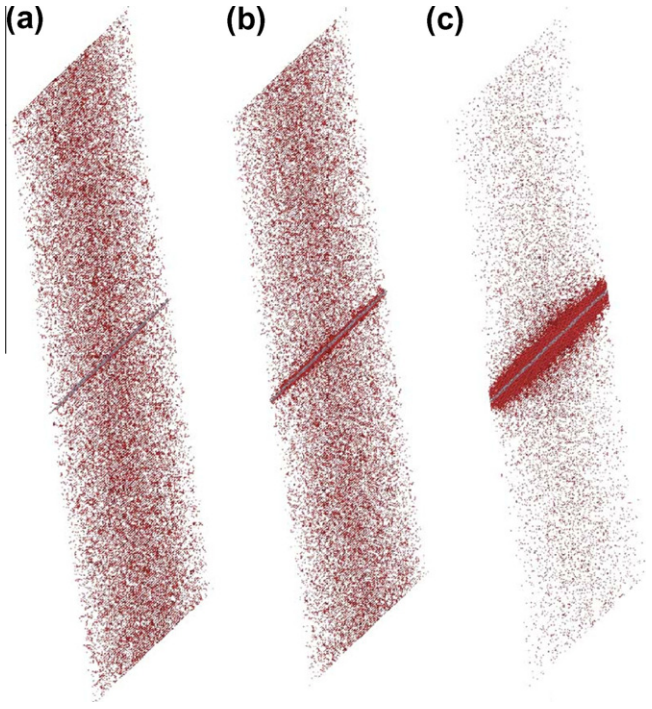

Fig. 6. Evolution of an undersaturated A–B alloy under irradiation at 800 K and 10^{-6} dpa s^{-1} ($C_B = 0.05$. solubility limit $C_{eq} = 0.08$), in a case where B atoms diffuse more slowly than A atoms by the vacancy mechanism, more rapidly by the interstitial mechanism. Microstructures at: (a) 2.46 10^{-3}, (b) 2.0 10^{-2} and (c) 1.20 dpa. Due to the radiation induced segregation, a continuous layer of B rich phase forms and grows at the point defect sink, as the irradiation dose increases [38]. Only B atoms are shown (red dots), the sink sites are in blue. (For interpretation of the references to colour in this figure legend, the reader is referred to the web version of this article.)

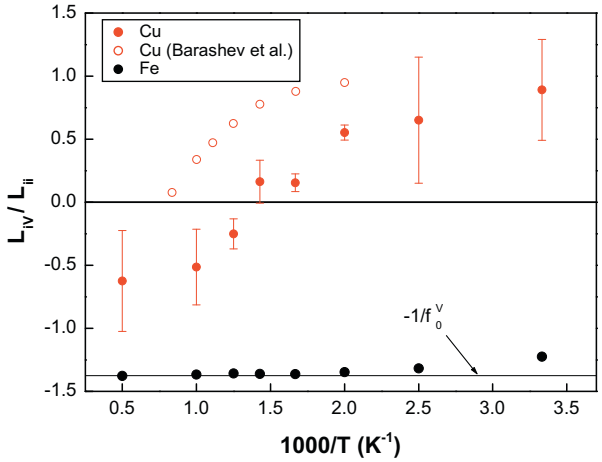

Fig. 7. Temperature dependence of the iron–vacancy and copper–vacancy phenomenological coefficients L_{iV} (normalized by the diagonal coefficients L_{ii}) measured in AKMC simulations [49]. Comparison with the previous study by Barashev and Arokiam [52].

3.3.2. Formation of point defect and solute cluster–cascade effects

The microstructure evolution of multicomponent Fe–CuMnNiSi alloys (with the same composition as in Section 3.2) has been studied under irradiation at 300 °C [39]. The first simulations have been performed at very high radiation fluxes (up to 10^{-1} dpa s^{-1}) in order to test the model. A rigid bcc lattice of 100 unit cells in each of the three space directions with periodic boundary conditions along the x and y axes and absorbing surfaces along z was used. The irradiation is simulated by introducing Frenkel pairs or cascade debris provided by Stoller [57] to simulate either an electron or a neutron irradiation. A total displacement dose of 2.5×10^{-3} dpa at a flux equal to 10^{-1} dpa s^{-1} was reached for the simulation involving Frenkel pairs. For the 20 keV cascades debris irradiations, a dose of 8.2×10^{-3} dpa was reached at a flux of 1 dpa s^{-1}, as well as a dose of 4×10^{-4} dpa associated with a flux of 1.6×10^{-6} dpa s^{-1}. The accumulated displacement per atom (dpa) is calculated using the NRT formula, which gives for the number of dpa per cascade:

$$n_{\mathrm{dpa}} = 0.8\frac{E_{\mathrm{MD}}}{2E_d}, \tag{4}$$

where E_{MD} is the damage energy, i.e. the fraction of the energy of the particle transmitted to the primary knock-on atom as kinetic energy and that is not absorbed by electronic excitation, equivalent to the energy by which the input cascade had been initiated in the MD simulation and E_d is the displacement threshold energy (40 eV). The contribution of a 20 keV cascade to the dpa is 200. In the case of electron irradiation simulation, Frenkel pairs are introduced randomly in the simulation box according to a certain dose rate. The contribution of a Frenkel pair to the dpa is 1.

The results of these first simulations indicate that the cluster distribution strongly depends on the radiation flux and point defect formation mechanism. As the time depends on the different events which have taken place in the simulation box, it is difficult to obtain snapshots at exactly the same time (or the same dose) in

the different simulations. However, the trends are quite clear. With 20 keV cascades and the highest radiation flux (Fig. 8b), the density of point defect clusters is extremely high (1×10^{27} m^{-3}) with clusters of 24 interstitials and 18 vacancies maximum. The point defect cluster densities observed with 20 keV cascades and the lowest radiation flux (Fig. 8c) or with a homogeneous Frenkel pair production and the highest radiation flux (Fig. 8a) are similar (the order of magnitude is 10^{23} m^{-3}). The clusters are bigger with the homogeneous Frenkel pair production, because cascades favour the formation in very localized area of small, stable and immobile (according to the model) clusters.

Point defect clusters seem to act as nuclei for the precipitation as solute atoms aggregate with them and decorate them. Illustrations of some point defect–solute complexes, which contain a vacancy rich core, are given in Fig. 9. For each irradiation, interstitial–solute complexes are smaller and mainly associated with Mn atoms. The percentage of solute atoms in clusters (not considering which other solutes belong to the cluster) compared to the initial distribution is also reported for each irradiation in Fig. 10. Cu is always the solute atom which precipitates the most. Mn precipitates more under cascade flux than under Frenkel pair flux. As could be expected from the stability of the mixed Fe–Mn dumbbell (Table 3), Mn precipitation is favoured by the presence of interstitial atoms. Ni, Mn and Si clustering also depends on the irradiation conditions (Fig. 10). First results are in qualitative agreement with experimental data: under electron irradiation, Si remains in solid solution [58], while under neutron irradiation Ni and Mn segregate with Cu clusters [59,60].

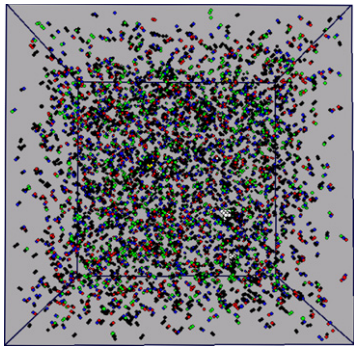

(a) Frenkel pair flux – 10^{-1} dpa.s^{-1} – 2.5×10^{-3} dpa

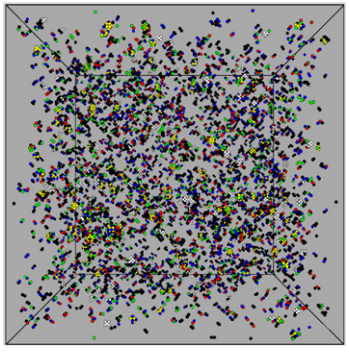

(b) 20 keV cascade flux – 1 dpa.s^{-1} – 8.2×10^{-3} dpa

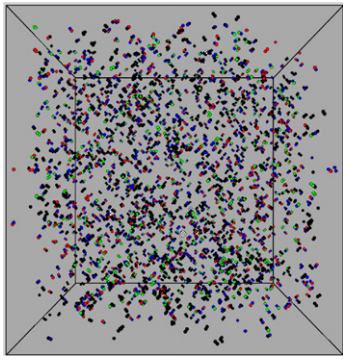

(c) 20 keV cascade flux – 1.6×10^{-6} dpa.s^{-1} – 4×10^{-4} dpa

Fig. 8. Microstructures obtained after irradiations of a dose of 2.5×10^{-3} dpa under Frenkel pair flux (a), 8.2×10^{-3} dpa under high 20 keV cascade flux (b) and 4×10^{-4} dpa under low 20 keV cascade flux (c). Only solute atoms in clusters of at least to two atoms and point defects are represented. Cu atoms are red, Ni green, Mn black, Si blue, vacancies yellow and Fe interstitials white. (For interpretation of the references to colour in this figure legend, the reader is referred to the web version of this article.)

4. Beyond rigid lattice approximations

4.1. Interatomic potentials versus ab initio for AKMC applications

The energy barriers that contain most of the physical information included in an AKMC model are, as mentioned, functions of the chemical environment and also of the local strain field. Ideally, they should be calculated on-the-fly using a reliable cohesive model including relaxation but, as discussed previously and in Ref. [44], the computational cost of it is too high to be feasible, except for limited applications, even using an interatomic potential. The way to follow is therefore to substitute the oversimplified, although efficiently evaluated, heuristic expressions of Appendix A by better ones. These should be able to reproduce both the extremely complex dependence on the chemical environment and the effect of the strain field.

It has been clearly shown that the heuristic expressions of Appendix A are inadequate to reproduce quantitatively the dependence of the energy barriers on the local chemical environment. The kinetic Ising, or FISE, model postulates a strict linearity between energy change due to the transition and energy barrier that represents only a very rough approximation [23]. Moreover, it is well-known that the (free) energy difference between two thermodynamic states determines the possibility of a transition, but cannot tell anything about its kinetics. Thus, the linear correlation between barriers and energy difference has in fact no solid bases. On the other hand, broken-bond methods lead necessarily, by the fact of being rigid lattice, pair-energy expressions, to a discretization of the possible saddle-point energy values, which cannot match the complexity of the actual configuration-dependence of the energy barrier [23]. This limits the capability of these expressions to be extrapolated beyond reference cases. The advantage of these expressions is, however, that only a few parameters need to be fitted, thereby providing the possibility of using directly *ab*

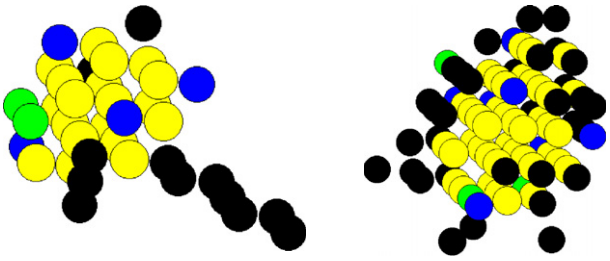

High 20 keV cascade debris flux Frenkel pair flux

Fig. 9. Illustrations of the biggest point defect – solute complexes formed during the high 20 keV cascade debris flux and the Frenkel pair flux. The vacancies are yellow, Mn is black, Ni green and Si are blue. (For interpretation of the references to colour in this figure legend, the reader is referred to the web version of this article.)

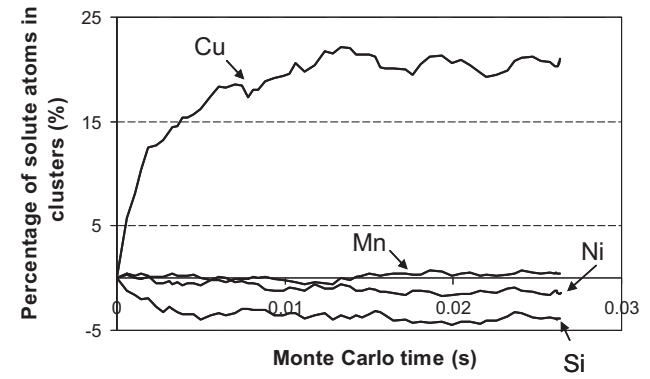

(a) Frenkel pair flux

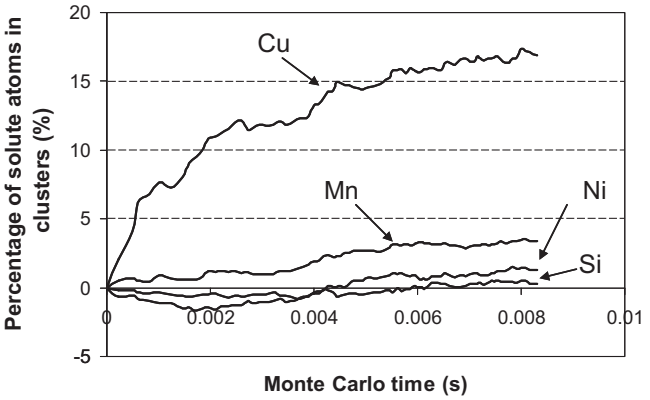

(b) High 20 keV cascade debris flux

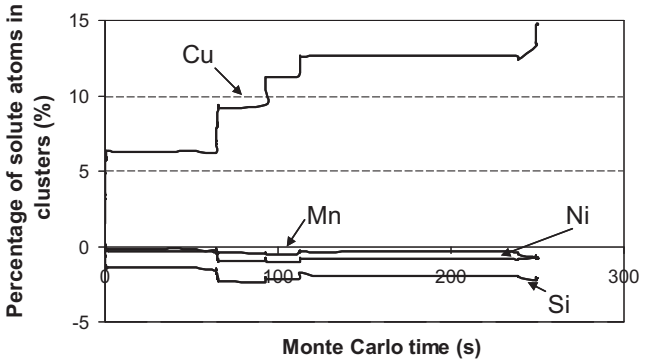

(c) Low 20 keV cascade debris flux

Fig. 10. Evolution of the percentage of solutes involved in clusters (with a critical size equal to 2) compared to the initial distribution as a function of the Monte Carlo time for the three irradiation conditions presented in Fig. 8.

initio reference data for this purpose. This allows in particular key thermodynamic quantities to be properly reproduced. However, it is unlikely that a new set of *ab initio* barriers, not used for the fitting, will be properly reproduced by the model; or at least it will strongly depend on the system and on the specific configuration whether good agreement is found or not. In addition, the *ab initio* calculations themselves, being limited to small systems, cannot account for long range elastic effects. For Fe–Cu alloys it has been for example estimated that, in the vicinity of a Cu precipitate, a proper calculation of the energy barrier for the exchange of a vacancy with a neighbouring atom should, in order to be fully accurate, include the effect of atoms as far as 8th nearest neighbour distance, or beyond [61]. This is due not really to the chemical influence of far-away atoms, but mainly to the strain field created by the nearby precipitate. Heuristic rigid-lattice expressions for the energy barriers, even though fitted to relaxed *ab initio* data, have no hope to be sensitive to any effect of this type.

There is, therefore, a double problem to be solved in order to improve the reliability of the expressions for the energy barriers to be used in AKMC models. They should be robust enough to be extrapolated to any local chemical configuration and should include relaxation effects in a proper way. The former calls for the use of a large set of examples against which the expressions should be not only fitted, but also validated. The latter requires large systems to be studied. For both purposes, *ab initio* calculations are currently not viable and the choice of an interatomic potential becomes the only possible one. If, however, the used expressions turn out to be accurate well beyond the fitting range (see next section), the gain is evident.

The question about the reliability of the method is then shifted to evaluating the reliability of the interatomic potential, where all the effort of reproducing *ab initio* reference data has to go. At any rate, even though, despite all efforts, the results provided by the potential turned out to be in some cases well apart from *ab initio* validation data, the advantage remains that an interatomic potential can be used for a wide range of studies, e.g. using molecular dynamics. Thus, if nothing else, a rigorous AKMC method relying on an interatomic potential can be seen, within its inherent limitations, as a consistent extension to larger time scales of studies performed by molecular dynamics in the same system.

Having in mind the large responsibility given to an interatomic potential in a framework of this type, a new Fe–Cu interatomic potential was developed within the Project, expressly conceived to provide a reliable cohesive model for fast and accurate calculations of a large number of energy barriers, having in mind AKMC applications [62,63]. For the pure elements, Fe and Cu, the most advanced potentials currently available were used. The fitting of the cross part was performed by using phase diagram points as reference data. In this way, a potential providing a solubility limit for Cu in Fe (and Fe in Cu) in close agreement with experimental measurements was produced. In addition, the potential was fitted to Cu–Cu and Cu–vacancy binding energies consistent with *ab initio* indications [64]. Finally, control was exerted on the vacancy migration energy barriers in the presence of a Cu atom, so as to approach the *ab initio* values and to provide a vacancy dragging effect (motion of the Cu–vacancy pair as a whole), as suggested by both experimental [65] and theoretical studies [52] and hitherto not reproduced by any FeCu potential. Such a potential is deemed to represent a good basis to fit advanced regression methods to predict energy barriers as function of the chemical environment, including relaxation effects.

4.2. Artificial intelligence regression of interatomic potential energy barriers

Regression methods that naturally lend themselves for the task of finding out how the energy barriers depend on the local chemical and elastic environment, given a reference cohesive model such as an interatomic potential, are for example based on the use of artificial intelligence tools, especially neural networks. Early attempts with genetic algorithms [66] and cluster expansion approaches [67] either failed or proved much less flexible and promising than using neural networks. The procedure is the following. A large number (on the order of a one hundred thousand) of energy barriers, for different (*a priori* randomly chosen) local environments, is rigorously calculated using a sufficiently reliable interatomic potential by means of the NEB method. This method has the advantage, compared to the cheaper drag method, of being of more general application (in the future it could be used to calculate energy barriers for self-interstitials as well), while being specific

for a transition between two known states, as is the case in an AKMC step. The local environment is coded by assigning an on-site variable to each lattice site contained in a reference volume around the migrating defect during the transition: the value of the on-site variable changes depending on the chemical/defect species sitting there. According to how many neighbour shells are included in the reference volume, the barrier is said to be calculated in 1st nearest neighbour (1nn), 2nn, . . . , *X*nn approximation. The number of on-site variables increases very rapidly with the extension of the reference volume: see Fig. 11 for the exchange between an atom and a vacancy on the bcc lattice. In practice, the local environment turns out to be coded as a vector of numbers, to which only one energy barrier value (calculated including relaxation effects) corresponds. The thereby tabulated barriers are divided in two sets: a training set and a validation set. The training set is used to provide examples of local environments (in terms of on-site variables) and corresponding energy barriers from which the neural network can learn and find the logic, thereby producing an advanced regression of barriers as functions of the environment. The validation set is used to test *a posteriori* the capability of extrapolation of the neural network to never-seen-before cases. The choice of the architecture of the neural network is described and discussed in Ref. [67], but a more elaborated training scheme, that is suitable for problems where many atomic sites must be taken into account, is briefly described in Ref. [68]. Fig. 12 shows the correlation of predicted versus calculated values in the case of an Fe and a Cu atom exchanging position with a vacancy, in 8nn approximation, where the local environment is defined by differently distributed Fe and Cu atoms. It can be seen that the performance of the neural network is amazingly good. It should be noted that there are 2^{143} possible local chemical configurations and that it is materially impossible to calculate all of them. What, however, is striking, is that training the neural network on a reduced number of them (a few tens of thousands) seems to be sufficient in order to have a satisfactory prediction for any number of never-seen-before configurations, randomly chosen among the 2^{143} possible ones. Increasing the level of the approximation (from 1nn to *X*nn) not only does not prevent the neural network from converging, but in fact improves its capability of extrapolation.

Once the neural network is trained, it is sufficient to plug it to the AKMC code to work as on-demand provider of barriers as functions of the local environment. An example of the application of this method to study the precipitation of Cu in Fe, using the potential described in the previous section [62,63], is given in Fig. 13 [61].

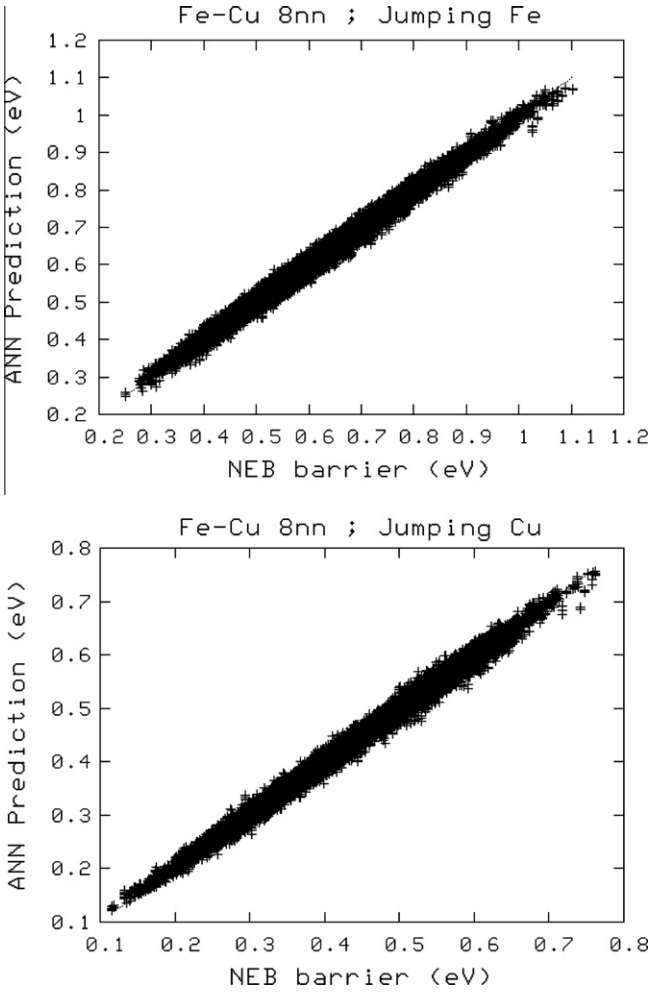

Fig. 12. Artificial Neural Network quality of predictions for the vacancy migration energy in an Fe–Cu alloy. The 8 nn are taken into account in the regression, corresponding to 143 input variables. The average errors are 1.1% and the correlation coefficients R^2 are 0.997.

The AKMC model has been validated by building the phase diagram that the model predicts. The model can be said to be accurate if it reproduces the same phase diagram as the interatomic potential

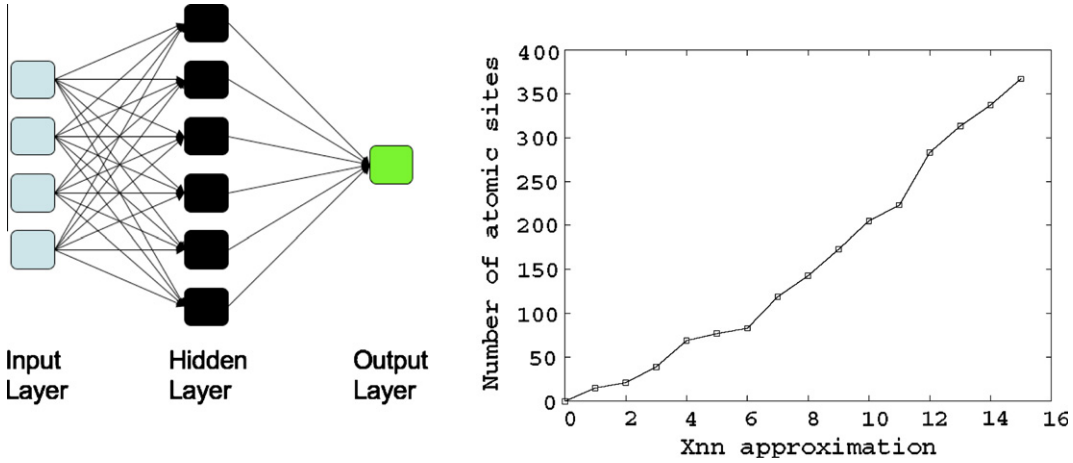

Fig. 11. (left) Artificial Neural Network, used to predict the vacancy migration energy as calculated by the NEB method. The inputs, strings of integers representing the local atomic configuration, are propagated from the left to the right of the network, through many simple processing units arranged in different layers. The final layer of the network counts only one node, whose output is the prediction of the vacancy migration energy. (right) Evolution with the number of shells of close atomic neighbours included in the local atomic configuration, of the number of corresponding atomic sites (i.e. the number of ANN input variables).

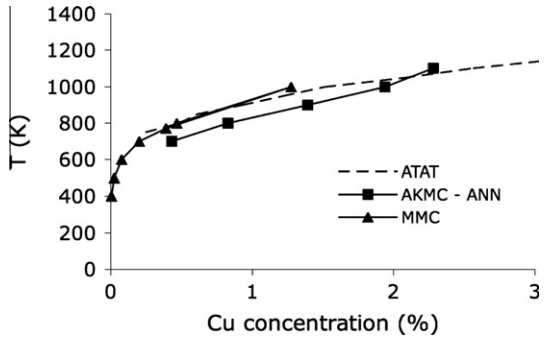

Fig. 13. Fe–Cu phase diagram predicted by different methods, all in a fully bcc framework. ATAT: phase boundaries obtained from rigid lattice Monte Carlo simulations in the semi-grand canonical (transmutation) ensemble on the basis of the Fe–Cu interatomic potential. MMC: rigid lattice Metropolis MC method. AKMC-ANN: Atomistic Kinetic MC method using ANN to predict the migration energy barriers, i.e. taking static relaxation effects into account.

(it cannot do any better than the potential itself). Fig. 13 compares the points forming the line that separates the region of full solubility from the region of phase separation, as found in a Metropolis MC study using the mentioned interatomic potential and with the ATAT package (rigid lattice Monte Carlo simulations in the semi-grand canonical ensemble), with the points obtained using the neural-network-based AKMC model. It can be seen that the sets of points can be interpolated by similar curves. The difference in the predictions of the models can be explained by the fact that static relaxation is taken into account in the energy barriers predicted by the ANN, whereas the MMC method and the ATAT package work in an entirely rigid lattice.

A study of the process of Cu precipitation in Fe under thermal ageing, conducted with the neural-network based technique, is reported in Ref. [61]. In this study, results comparable with those shown on Fig. 3 using the broken-bond model where obtained. Better results could not be obtained, because those of Fig. 3 are already good ones. The real advantage of this method is that it opens the way to a proper calculation of barriers for not only vacancy jumps, but also SIAs, as functions of their orientation and the orientation of nearby SIAs, thereby possibly allowing SIA clustering to be more properly treated in an AKMC scheme. The extension to SIAs is, however, not trivial, mainly because of the difficulty of building the training set. In short, the problem is that *a priori* the neural network should be able to provide correct barriers for any transition between any two possible states: if the barrier is high the transition will be unlikely, if it is low it will be frequent, but all cases need to be included. When the local environment is defined by chemical species, this is not a problem, because all configurations are physically possible. Not so when the local environment is defined by SIAs: the interaction between strain fields around them determines indeed that some configurations are simply impossible and forcing them to occur for training purposes produces unphysical results, by which the neural network is "confused", thereby failing to find any logic in the data. It becomes therefore necessary first of all to classify the configurations into possible and impossible ones, before proceeding with the calculation of the barriers and training the neural network on them. Developments along this line are currently ongoing.

5. Conclusions

AKMC simulations benefit from several advantages to deal with microchemical and microstructural changes controlled by point defect diffusion in alloys under irradiation:

- By comparison with rate theory and OKMC methods, which cannot for example describe all possible fluctuations of local composition (especially in concentrated and multi component alloys), they take into account the full atomic distribution, i.e. they do not need any special hypothesis on the phases that can appear, on the shape or the microstructure of precipitates and clusters that are formed. They are therefore especially suitable to trace the microchemical evolution in detail. The only limitation in this sense – for the time being – is the impossibility of describing the formation of phases with different crystallographic structures.
- By comparison with phase-field and mean-field model, they take into account the exact dependence of the migration barriers on the local configuration (for a given model of the barriers), as well as the correlations between successive point defects jumps, which both control the diffusion properties of the system and the microchemical evolution. They also include thermal fluctuations that control the nucleation processes.

Exploiting these advantages, AKMC simulations have been used in the Perfect project to study point-defects and solute clustering, in binary and multicomponent iron based alloys, during thermal ageing and under irradiation.

The main progresses in the program have been:

- The selection of better AKMC parameters, mainly due to the extensive use of *ab initio* calculations of formation energies and migration barriers, as reference data for the fitting procedure.
- A better understanding of the key parameters controlling the kinetics of copper precipitation during thermal ageing and a quantitative agreement with experiments, at least for short times.
- The development of AKMC codes including interstitials with realistic dumbbell configurations and jump mechanisms (iron rich bcc alloys), and preliminary studies of the consequences of such mechanisms on the microstructure evolutions of binary and multi component alloys (Radiation Induced Segregation, solute and point defect clustering).
- A better treatment of point defect concentrations and time scales.

In addition, to go beyond the rigid lattice approximation and deal with atomic relaxation and long range elastic interactions, a new methodology has been developed for the prediction of migration barriers. It is based on the use of neural networks to "find the logic" behind many examples calculated using an empirical potential, including the effect of full atomic relaxations. The method has been successfully applied to the vacancy diffusion mechanisms, and to copper precipitation kinetics. The application to the SIA diffusion mechanism is in progress.

Each AKMC "recipe" has advantages and shortcomings, as has been discussed. It is then important to develop in parallel models based on different strategies, in order to be able – for a given application – to identify the key parameters driving the evolution of the system, which may be differently reproduced by different methods. This way of proceeding may be also a way of quantitatively assessing the uncertainties behind these methods (otherwise very difficult to estimate) and of achieving a better physical understanding, beyond the specific result that each method provides.

Among the main disadvantages of AKMC simulations remains the fact that they are time consuming and thus limited to the early stages of microchemical evolutions, especially when strong point-defect/solution correlations and trapping effects exist. The link with simpler and more rapid approximations (OKMC, rate theory) is therefore highly desirable. Unfortunately, it is far from being

straightforward, especially under irradiation and in multicomponent alloys, mainly because the composition and the structure of the phases and clusters that appear during the evolution of the system can be very complex and are not simply predictable from equilibrium consideration.

Finally it is worth noting that some important mechanisms are for the time being very difficult to include in AKMC methods, e.g. the loss of coherency during precipitation processes, or the one dimensional, almost athermal, migration of small SIA clusters, which has been revealed by MD simulations. Such features could strongly affect the kinetic pathways, and their integration in AKMC models is a key issue for future work.

Acknowledgments

The authors gratefully acknowledge all those who have contributed to the articles discussed here, especially G. Cerchiara, F. Djurabekova, R. Domingos, and Chu-Chun Fu. This work is part of the European PERFECT project and supported by the European Commission (FI60-CT-2003-508840). Part of this work was performed using HPC resources from GENCI-CINES (Grant 2009-x2009096020).

Appendix A. Models for migration barriers

In the development of diffusion model and Monte Carlo algorithms, it is important to distinguish the *energy difference* between an initial configuration i and a final configuration f ($\Delta E = E_f - E_i$) and the *migration barrier* between the two configurations ($\Delta E_m^{i\to f} = E_{SP} - E_i$ and $\Delta E_m^{f\to i} = E_{SP} - E_f$). The first one controls the equilibrium probabilities of the configurations, while the migration barriers control both the equilibrium and the kinetic properties. Two methods have been used in the framework of the Project to compute the migrations barriers of the vacancies as well of the dumbbells:

The Kinetic Ising Model (or FISE model in Ref. [21]). The saddle-point energy is estimated by:

$$E_{SP} = \frac{E_i + E_f}{2} + Q, \tag{A1}$$

which leads to

$$\Delta E_m^{i\to f} = \frac{E_f - E_i}{2} + Q, \tag{A2}$$

where $E_f - E_i$ corresponds to the balance of bonds between stable lattice positions, created and destroyed during the jump and Q is a constant parameter, usually fitted on diffusion coefficients in pure metals.

Saddle-Point Energy model. For e.g. an A–V exchange: the migration barrier is written:

$$\Delta E_m^{A} = E_{SP} - E_i = e_{SP}^{A} - \sum_i \varepsilon_{Ai} - \sum_j \varepsilon_{Vj} \tag{A3}$$

where the sums run over the bonds broken around A and V in their initial positions and e_{SP}^{A} is the interaction between A and its neighbours, when it is at the saddle-point. This parameter can be a constant only dependant of the nature of A (as in Ref. [15] or [21]) or computed as a sum of effective interactions between the SP and the neighbouring atoms, e.g.: $e_{SP}^{A} = \sum_i \varepsilon_{iA}^{SP}$ [11,16].

The first model imposes a linear relation between the height of the migration barriers and the energy difference between stable positions which is questionable [34,44]. However, it allows the migration barriers to be evaluated without computing the energy at the saddle-point, using for example an empirical interatomic potential and then including chemical interactions up to a much larger distance than just first and second nearest neighbours (to where broken-bond models are typically limited) and even strain effects.

The second model has the advantage of not imposing a relation between the high of the barrier and the energy of the final state, which is in agreement with the theory of thermally activated processes. It also gives more flexibility to fit the dependence on the barriers on the atomic configurations from empirical potentials [11] or *ab initio* calculations [16]. But it is also limited to simple interactions on a rigid lattice, and the extrapolation beyond the range of fitting is questionable.

For practical purposes, the choice of the most appropriate model can depend of the system which is considered and the actual capability of both models to properly allow for the effect of the local environment remains limited, at least when only pair interactions are used.

References

[1] D.J. Bacon, F. Gao, Y.N. Osetsky, J. Nucl. Mater. 276 (2000) 1.
[2] L. Malerba, G. Ackland, C.S. Becquart, G. Bonny, et al., J. Nucl. Mater. 406 (2010) 7.
[3] C.S. Becquart, A. Barbu, J.-L. Bocquet, M.J. Carturla, J. Nucl. Mater. 406 (2010) 39.
[4] M. Athenes, P. Bellon, G. Martin, Deffect Diffus. Forum 143 (1997) 297.
[5] M. Athenes, P. Bellon, G. Martin, Acta Mater. 48 (2000) 2675.
[6] M. Athenes, P. Bellon, G. Martin, F. Haider, Acta Mater. 44 (1996) 4739.
[7] P. Binkele, S. Schmauder, Z. Metallkd. 94 (2003) 858.
[8] E. Clouet, L. Lae, T. Epicier, W. Lefebvre, et al., Nat. Mater. 5 (2006) 482.
[9] E. Clouet, M. Nastar, in: P.E.A. Turchi et al. (Eds.), Complex Inorganic Solids – Structural, Stability, and Magnetic Properties of Alloys, Springer Verlag, New York, 2005, p. 215.
[10] E. Clouet, M. Nastar, C. Sigli, Phys. Rev. B 69 (2004).
[11] Y. Le Bouar, F. Soisson, Phys. Rev. B 65 (2002) 094103.
[12] Z.G. Mao, C.K. Sudbrack, K.E. Yoon, G. Martin, et al., Nat. Mater. 6 (2007) 210.
[13] C. Pareige, F. Soisson, G. Martin, D. Blavette, Acta Mater. 47 (1999) 1889.
[14] C. Pareige-Schmuck, F. Soisson, D. Blavette, Mater. Sci. Eng. A 250 (1998) 99.
[15] F. Soisson, A. Barbu, G. Martin, Acta Mater. 44 (1996) 3789.
[16] F. Soisson, C.-C. Fu, Phys. Rev. B 214102 (2007).
[17] F. Soisson, G. Martin, Phys. Rev. B 62 (2000) 203.
[18] E. Vincent, C.S. Becquart, C. Domain, J. Nucl. Mater. 351 (2006) 88.
[19] E. Vincent, C.S. Becquart, C. Domain, Nucl. Instr. Methods Phys. B 255 (2007) 78.
[20] S. Schmauder, P. Binkele, Comput. Mater. Sci. 24 (2002) 42.
[21] E. Vincent, C.S. Becquart, C. Pareige, P. Pareige, et al., J. Nucl. Mater. 373 (2008) 387.
[22] O. Khrushcheva, E.E. Zhurkin, L. Malerba, C.S. Becquart, et al., Nucl. Instr. Methods Phys. B 202 (2003) 68.
[23] F.G. Djurabekova, L. Malerba, C. Domain, C.S. Becquart, Nucl. Instr. Methods Phys. B 255 (2007) 47.
[24] C. Domain, C.S. Becquart, J.-C.V. Duysen, Mater. Res. Soc. Symp. Proc. 540 (1999) 643.
[25] L. Malerba, C.S. Becquart, M. Hou, C. Domain, Philos. Mag. 85 (2005) 417.
[26] B.D. Wirth, G.R. Odette, Mater. Res. Soc. Symp. Proc. 540 (1999) 637.
[27] D. Gendt, P. Maugis, G. Martin, M. Nastar, et al., Diffus. Mater Dimat. 194-1 (Pts 1 & 2) (2001) 1779.
[28] C. Hin, Y. Bréchet, P. Maugis, F. Soisson, Acta Mater. 56 (2008) 5653.
[29] C. Hin, Y. Bréchet, P. Maugis, F. Soisson, Acta Mater. 56 (2008) 5535.
[30] E. Vincent, C.S. Becquart, C. Domain, J. Nucl. Mater. 359 (2006) 227.
[31] C. Domain, C.S. Becquart, Phys. Rev. B 65 (2001) 024103.
[32] C.C. Fu, F. Willaime, P. Ordejon, Phys. Rev. Lett. 92 (2004) 175503.
[33] C.S. Becquart, C. Domain, Phys. Status Solidi B 247 (2010) 9.
[34] F.G. Djurabekova, R. Domingos, G. Cerchiara, N. Castin, et al., Nucl. Instr. Methods Phys. B 255 (2007) 8.
[35] W.M. Young, E.W. Elcock, Proc. Phys. Soc. Lond. 89 (1966) 735.
[36] A.B. Bortz, M.H. Kalos, J.L. Lebowitz, J. Comput. Phys. 17 (1975) 10.
[37] A. Chatterjee, D.G. Vlachos, J. Comput-Aid. Mater. 14 (2007) 253.
[38] F. Soisson, J. Nucl. Mater. 349 (2006) 235.
[39] E. Vincent, C.S. Becquart, C. Domain, J. Nucl. Mater. 382 (2008) 154.
[40] F. Soisson, C.-C. Fu, Solid State Phenom. 139 (2008) 107.
[41] E. Clouet, Ph.D thesis, Ecole Centrale, Paris, 2004.
[42] F. Soisson, C.-C. Fu, Solid State Phenom. 129 (2007) 31.
[43] A. Finel, in: P.E.A. Turchi, A. Gonis (Eds.), Phase Transformations and Evolution in Materials, TMS, Warrendale, 2000, p. 371.
[44] J.L. Bocquet, Defects and Diffusion in Metals: An Annual Retrospective Iv 203-2 (2002) 81.
[45] H. Gupta, R. Weinkamer, P. Fratzl, J.L. Lebowitz, Acta Mater. 49 (2001) 53.
[46] G. Henkelman, G. Jóhannesson, H. Jónsson, in: S.D. Schwartz (Ed.), Progress on Theoretical Chemistry and Physics, Kluwer Academic Publishers, 2000, p. 269.
[47] G.R. Odette, G.E. Lucas, JOM 53 (2001) 18.
[48] P.J. Othen, M.L. Jenkins, G.D.W. Smith, Philos. Mag. A 70 (1994) 1.
[49] G. Salje, M. Feller-Kniepmeier, J. Appl. Phys. 45 (1977) 1833.
[50] M. Perez, F. Perrard, V. Massardier, X. Kleber, et al., Philos. Mag. 85 (2005) 2197.

[51] E. Vincent, C.S. Becquart, C. Domain, Nucl. Instr. Methods Phys. B 228 (2005) 137.
[52] A.V. Barashev, A.C. Arokiam, Philos. Mag. Lett. 86 (2006) 321.
[53] J.M. Roussel, P. Bellon, Phys. Rev. B 6318 (2001) 184114.
[54] C.L. Liu, G.R. Odette, B.D. Wirth, G.E. Lucas, Mater. Sci. Eng. A 238 (1997) 202.
[55] K.C. Russell, Prog. Mater. Sci. 28 (1984) 229.
[56] A.R. Allnatt, A.B. Lidiard, Atomic Transport in Solids, Cambridge Univ. Press, Cambridge, 1993.
[57] R.E. Stoller, J. Nucl. Mater. 276 (2000) 22.
[58] B. Radiguet, Ph.D thesis, Université de Rouen, 2004.
[59] J.T. Buswell, C.A. English, M.G. Hetherington, W.J. Phythian, et al., in: N.H. Packan, R.E. Stoller, A.S. Kumar (Eds.), 14th International Symposium on Effects of Radiation in Materials, ASTM-STP, Andover, Massachusetts, 1990, p. 127.
[60] M.K. Miller, B.D. Wirth, G.R. Odette, Mater. Sci. Eng. A 353 (2003) 133.
[61] N. Castin et al., in: Proceedings of the 9th International Conference on Computer Simulation of Radiation Effects in Solids, COSIRES, Beijing, 2008.
[62] L. Malerba, R.C. Pasianot, SCK-CEN Report ER-6, SCK-CEN, Mol, 2006.
[63] R.C. Pasianot, L. Malerba, J. Nucl. Mater. 360 (2007) 118.
[64] C.S. Becquart, C. Domain, Nucl. Instr. Methods Phys. B 202 (2003) 44.
[65] Y. Nagai, Z. Tang, M. Hassegawa, T. Kanai, et al., Phys. Rev. B 6313 (2001).
[66] R. Domingos, G. Cerchiara, F. Djurabekova, L. Malerba, in: D. Ruan et al. (Eds.), Applied Artificial Intelligence – Proceedings of the 7th International FLINS Conference, World Scientific, 2006.
[67] N. Castin, R.P. Domingos, L. Malerba, IJCIS 1 (2008) 340.
[68] N. Castin, L. Malerba, G. Bonny, M.I. Pascuet, et al., Nucl. Instr. Methods Phys. B 267 (2009) 3002.